

# MAG.I.C.AL.—A Unified Methodology for Magnetic and Inertial Sensors Calibration and Alignment

Konstantinos Papafotis, *Student Member, IEEE*, and Paul P. Sotiriadis, *Senior Member, IEEE*

**Abstract**—This paper introduces the MAGnetometer-INertial sensors Calibration and ALignment (MAG.I.C.AL.) methodology for unified calibration and joint axes alignment of three-axis magnetometer, three-axis accelerometer, and three-axis gyroscope. MAG.I.C.AL. compensates for all linear time-invariant distortions such as scale-factor, cross-coupling, and offset, including the soft-iron and hard-iron distortions of the magnetometer. It introduces a new, computationally efficient, least-squares-based iterative algorithm for the calibration of the magnetometer and the accelerometer. It aligns their axes and introduces a new way to calibrate the gyroscope based on their joint data. MAG.I.C.AL. is implemented in a 15-step sequence achieving fast convergence and high accuracy without using any external piece of equipment and without requiring external attitude references. Simulation and experimental results using low-cost sensors are presented to support the accuracy, efficiency, and the applications of the algorithm.

**Index Terms**—Accelerometer, axes alignment, calibration, gyroscope, hard-iron, inertial sensors, joint calibration, magnetometer, navigation, soft-iron.

## I. INTRODUCTION

**I**NERTIAL sensors, accelerometers and gyroscopes, are combined with magnetometers in a wide range of applications. For example, in [1] and [2] the three sensors are combined in pedestrian navigation applications. Two heading estimation algorithms based on their joint data are presented in [3] and [4]. Many applications where the three sensors are combined can be found in the literature, from low-cost commercial systems to high-accuracy marine, aerospace and military systems.

Especially in the case of low-cost systems, micro-electro-mechanical (MEMS) inertial sensors are usually preferred due to their significantly lower cost and small size. However, a major disadvantage of MEMS inertial sensors is their large error characteristics [5]. So, in order to use them in applications where accuracy is important, such as navigation, a calibration procedure that compensates for the deterministic part of their error is required.

Manuscript received April 21, 2019; accepted May 9, 2019. Date of publication May 27, 2019; date of current version August 15, 2019. This work was supported by the Greece and the European Union (European Social Fund-ESF) through the Operational Programme “Human Resources Development, Education, and Lifelong Learning” in the context of the Project “Strengthening Human Resources Research Potential via Doctorate Research” under Grant MIS-5000432, implemented by the State Scholarships Foundation (IKY). The associate editor coordinating the review of this paper and approving it for publication was Dr. Jürgen Kosel. (*Corresponding author: Konstantinos Papafotis.*)

The authors are with the National Technical University of Athens, 15780 Zografou, Greece (e-mail: k.papafotis@gmail.com; pps@ieee.org).

Digital Object Identifier 10.1109/JSEN.2019.2919179

Similarly to the inertial MEMS sensors, low-cost magnetometers also suffer from significant measurement errors. Apart from the sensor’s manufacturing imperfections, the measured magnetic field is strongly distorted by nearby magnetic materials. Surrounding electronic components and the sensor’s enclosure are a common source of such distortions. Getting an accurate magnetic field measurement requires a calibration procedure to compensate for both sensor’s measurement error and the distortions caused by nearby objects.

In the case of low-cost inertial and magnetic sensors, factory calibration or after-production calibration using expensive equipment is not an option as it would raise the sensor’s cost significantly. Thus, a calibration method that is not based on any external equipment is highly preferred.

For 3-axis accelerometer calibration, most authors take advantage of the fact that the measured magnitude of the specific force is constant when the sensor is still, independently of its orientation. The work in [6] proposes an off-line calibration method based on maximum likelihood estimation. In [7] an algorithm based on least-square method is proposed. In [8] the authors propose a solution based on the Levenberg-Marquardt algorithm to improve the calibration accuracy. The authors in [9] use a nonlinear parameter estimator based on the unscented transformation to calculate the calibration parameters. In [10], calibration parameters are calculated by solving a nonlinear optimization problem.

Gyroscope calibration is a more complicated problem as no convenient rotation reference is available. Some authors use special equipment in order to calibrate a gyroscope [11]–[13]. In [14], the authors use the earth’s rotation as reference, an approach suffering from the MEMS gyroscope relatively high noise levels. In [15] the rotation of a calibrated accelerometer is used as a reference in a least squares problem formulation. Authors in [16] use a calibrated magnetometer in a Kalman filter estimation problem to calculate the calibration parameters.

For 3-axis magnetometer calibration, the magnetic field of the earth is most commonly used as reference. In [17]–[21] the authors derive the calibration parameters by solving a maximum likelihood estimation problem. A least-squares based iterative algorithm for magnetometer calibration is proposed in [22]. In [23], the authors formulate the magnetometer calibration as a state estimation problem which can be solved using Kalman filtering.

In most navigation or heading estimation applications the measurements of the three (accelerometer, gyroscope, magnetometer) are combined to give a more accurate result.

This gives rise to the need of alignment between the axes of the three sensors. In [24] and [25], magnetometer's axes are aligned with those of the accelerometer. The authors in [26] and [23] use a gyroscope to align magnetometer and inertial sensors. An algorithm for calibration and axes alignment between a gyroscope and an accelerometer is proposed in [27].

The calibration of inertial and magnetic sensors, and the alignment of their axes is required in all relevant applications. However, most of the previous works deal only with the calibration of either a single sensor or the alignment between a pair of them.

This work introduces the MAG.I.C.AL. methodology to jointly calibrate and align the axes of all three sensors (3-axis accelerometer, 3-axis gyroscope and 3-axis magnetometer) in a simple 15-steps sequence, achieving high accuracy without requiring any special piece of equipment.

Specifically, MAG.I.C.AL. calibrates the 3-axis accelerometer and the 3-axis magnetometer independently, aligns their axes and uses their calibrated measurements to accurately calibrate the 3-axis gyroscope without the need of a turn-table.

MAG.I.C.AL. introduces a new calibration algorithm for the magnetometer and the accelerometer, and, a new calibration approach and the corresponding algorithm for the gyroscope. MAG.I.C.AL. also improves in computational efficiency and convergence rate compared to existing techniques.

The paper is organized as follows. In sections II and III magnetometer and accelerometer calibration algorithms are described respectively. Section IV addresses the axes alignment between an accelerometer and a magnetometer. Section V describes the gyroscope calibration algorithm. In section VI, MAG.I.C.AL. methodology is described as a complete calibration and axes alignment procedure. Finally, evaluation of the proposed algorithm using experimental data and conclusions are presented in sections VII and VIII.

## II. MAGNETOMETER CALIBRATION

The 3-axis magnetometer's calibration is based on the fact that the measured magnitude of the magnetic field should be independent of the magnetometer's orientation. This is formulated as an optimization problem which is solved using a novel least-squares based iterative algorithm achieving fast convergence and computational efficiency.

### A. Hard-Iron and Soft-Iron Distortions

A magnetometer measures the strength and the direction of the local magnetic field. The measured field is a combination of the earth's magnetic field and an additive field created by magnetic objects attached to the same reference frame as the sensor. This additive field is called hard-iron distortion and causes a permanent bias in the sensor's output.

In addition, magnetometer's measurement is distorted by nearby materials attached to the sensor's frame that influence the magnetic field but don't generate a magnetic field themselves, most commonly metals. This type of distortion is called soft-iron distortion, and, along with the hard-iron distortion are the most important error contributors in the measurements.

### B. Measurement Model

Taking into account the hard-iron and soft-iron distortions which are the two dominant sources of distortion, the sensor's measurement can be modeled as [18], [21], [24], [28]

$$y_m = T_{sf} T_{cc} (T_{si} m + h_{hi}) + h_b + \varepsilon \quad (1)$$

where  $y_m$  is the  $3 \times 1$  measurement vector,  $T_{sf}$  is a  $3 \times 3$  diagonal matrix representing the linear scale-factor error,  $T_{cc}$  is a  $3 \times 3$  matrix representing the cross-coupling error which arises from the misalignment of the sensor's axes.  $T_{si}$  is a  $3 \times 3$  matrix representing the soft-iron distortion,  $m$  is the  $3 \times 1$  true magnetic field vector,  $h_{hi}$  is the  $3 \times 1$  bias vector due to the hard-iron distortion,  $h_b$  is the  $3 \times 1$  sensor's bias vector and  $\varepsilon$  is the measurement's random error.<sup>1</sup>

Setting  $T_m \triangleq T_{sf} T_{cc} T_{si}$  and  $h_m \triangleq T_{sf} T_{cc} h_{hi} + h_b$ , the magnetometer's measurement model becomes

$$y_m = T_m m + h_m + \varepsilon \quad (2)$$

### C. Calibration Algorithm

The purpose of the calibration algorithm is to estimate the calibration parameters  $T_m$  and  $h_m$  in order to minimize the measurement error  $\|\varepsilon\|$  while assuming a constant magnitude for the measured magnetic field. Thus, given  $N$  measurements, the problem of calibrating a magnetometer can be posed as the following optimization problem

$$\begin{aligned} & \underset{T_m, h_m}{\text{minimize}} \sum_{k=1}^N \|y_{mk} - T_m m_k - h_m\|^2 \\ & \text{subject to } \|m_k\| = 1, \quad k = 1, 2, \dots, N \end{aligned} \quad (3)$$

All norms in this paper are two-norms unless it is indicated otherwise. In (3), without loss of generality, we assume the magnitude of the magnetic field is one. A penalty function corresponding to (3) is

$$J = \sum_{k=1}^N \left[ \|y_{mk} - T_m m_k - h_m\|^2 + \lambda \left( \|m_k\|^2 - 1 \right)^2 \right] \quad (4)$$

where  $\lambda$  is a positive constant. It should be selected to balance the contribution of the two summands.<sup>2</sup>

Minimizing (4) using gradient descent or Newton-Raphson methods require a good initial estimate of the unknowns  $T_m$  and  $h_m$ , otherwise they are very slow in convergence, if they converge at all. Finding an initial estimate is not trivial due to the uncertainty of soft-iron and hard-iron distortions; the authors in [18] and [24] propose a linear least-squares problem in order to find one. In [22] a solution to (3) by means of iterations of a least-square problem is proposed which excels in computational efficiency and convergence.

Similarly to [22], we propose an iterative solution to (3) based on the solution of a linear least-squares problem. We start with rewriting (2) in matrix form for all measurements

$$Y = LG + E \quad (5)$$

<sup>1</sup> $\varepsilon$  is assumed to be a zero mean random variable.

<sup>2</sup>Typically it is selected to be in the order of  $\|T_m\|$ .

where

$$Y = [y_{m1} \ y_{m2} \ \dots \ y_{mN}], \quad L = [T_m \ h_m]$$

$$G = \begin{bmatrix} m_1 & m_2 & \dots & m_N \\ 1 & 1 & \dots & 1 \end{bmatrix} \quad \text{and} \quad E = [\varepsilon_1 \ \varepsilon_2 \ \dots \ \varepsilon_N]$$

The system (5) has  $3 \times N$  equations. Assuming an initial estimate of a full rank matrix  $G$ , every iteration of the algorithm begins with deriving  $T_m$  and  $h_m$  minimizing the total squared error  $\|E^T E\|_F^2$ . From least-squares method [29] we have

$$L = YG^T(GG^T)^{-1} \quad (6)$$

Using the updated values of  $T_m$  and  $h_m$  and (2) we define

$$\tilde{m}_k = T_m^{-1}(y_{mk} - h_m), \quad k = 1, 2, \dots, N \quad (7)$$

where we assume that  $T_m$  is invertible. This is a rational assumption as a non-invertible  $T_m$  would imply that not all three axes are expressed in the output of the sensor.

Since the magnitude of the magnetic field is independent of the measurement, and set to one for convenience, we update  $m_k$  as

$$m_k = \frac{\tilde{m}_k}{\|\tilde{m}_k\|} \quad (8)$$

As a metric of convergence we use the value of the penalty function  $J$  in (4).

The magnetometer calibration algorithm is summarized in Algorithm 1.

---

#### Algorithm 1: Magnetometer Calibration

---

- Step 1: Initialize  $m_k = \frac{y_{mk}}{\|y_{mk}\|}$ ,  $k = 1, 2, \dots, N$   
and form matrix  $G$
  - Step 2: Solve for  $L$  using least-squares:  
 $L = YG^T(GG^T)^{-1}$
  - Step 3: Extract  $T_m$  and  $h_m$  from  $L$
  - Step 4:  $\tilde{m}_k = T_m^{-1}(y_{mk} - h_m)$ ,  $k = 1, 2, \dots, N$
  - Step 5: Update  $G$  using  $m_k = \frac{\tilde{m}_k}{\|\tilde{m}_k\|}$ ,  $k = 1, 2, \dots, N$
  - Step 6: Calculate  $J$
  - Step 7: Repeat steps 2-6 until  $J$  is sufficiently small
- 

#### D. Recommended Calibration Procedure

The goal of the calibration procedure is to derive matrix  $T_m$  and vector  $h_m$  in (2) modeling the behavior of the magnetometer.

Assuming  $N$  magnetometer's measurements, we formulate a system of  $N$  equations of the form of (2). An intuitive way to calculate the minimum number  $N$ , required to derive the calibration matrix  $T_m$  and the offset vector  $h_m$ , is the following: matrix  $T_m$  and vector  $h_m$  are the same for all equations and thus they contribute 12 ( $3 \times 3 + 3 \times 1$ ) unknowns in total. For every measurement, the (unknown) magnetic field vector  $m$ , contributes another 3 unknowns. So, in total there are  $12 + 3N$  unknowns. Every measurement expressed in the form of (2), contributes 3 scalar equations. In addition, since

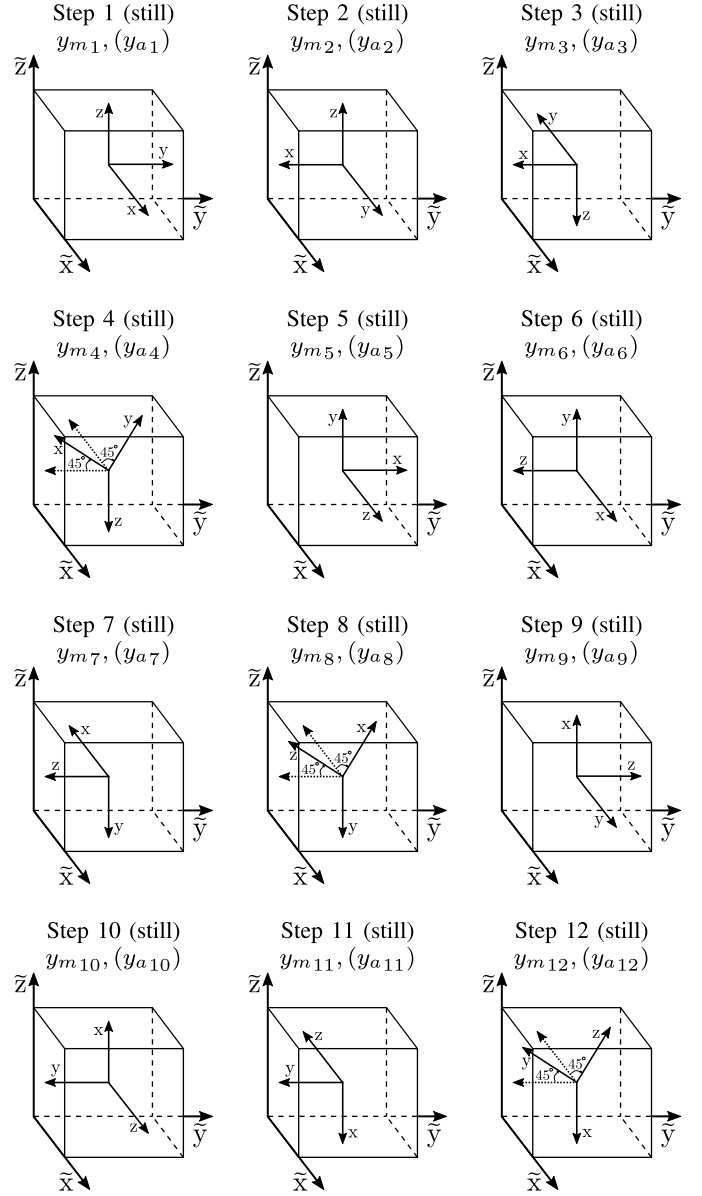


Fig. 1. Recommended sequence of approximate orientations for magnetometer calibration.

the magnetic field vector  $m$  is of unit norm, we get one more scalar equation for every measurement. So, in total we have  $3N + N$  equations. Balancing unknowns with equations gives a minimum  $N = 12$ .

To this end, we recommend the calibration procedure shown in Figure 1 where the sensor measures the magnetic field by being placed in 12 different approximate orientations. Specifically, in Figure 1, the  $(X, Y, Z)$  coordinate system denotes the sensor's body frame and the  $(\tilde{X}, \tilde{Y}, \tilde{Z})$  coordinate system denotes the calibration reference frame which is fixed. For each orientation, as shown in Figure 1, the respective  $y_{mk}$ ,  $k = 1, 2, \dots, 12$  is measured. Note that the steps in Figure 1 should not be confused with the steps of the Algorithm 1.

**Important Note:** The orientation of the sensor in meant to be **approximate**, no accuracy is needed. Orientation and

placement of the sensor can be done by hand with an accuracy of say  $+/- 15^\circ$  of Euler angle.

The described magnetometer calibration algorithm and procedure were tested on experimental data. The results of those tests are discussed in section VII.

### III. ACCELEROMETER CALIBRATION

The 3-axis accelerometer's calibration algorithm exploits the fact that measured magnitude of the specific force should be constant when the sensor is still, independently of the sensor's orientation.

#### A. Measurement Model

Accelerometer's measurement is modeled as [5], [30]

$$y_a = f + T_{sf}f + T_{cc}f + h_a + \varepsilon, \quad (9)$$

where  $y_a$  is the  $3 \times 1$  measurement vector,  $f$  is the  $3 \times 1$  true specific force vector,  $T_{sf}$  is a  $3 \times 3$  diagonal matrix representing the linear scale-factor error of the sensor,  $T_{cc}$  is a  $3 \times 3$  matrix representing the cross-coupling error,  $h_a$  is the  $3 \times 1$  accelerometer bias vector and  $\varepsilon$  is the sensor's random error.<sup>3</sup> Defining  $T_a \triangleq I_3 + T_{sf} + T_{cc}$ , where  $I_3$  is the  $3 \times 3$  identity matrix, (9) can be written as

$$y_a = T_a f + h_a + \varepsilon \quad (10)$$

#### B. Calibration Algorithm

A popular calibration approach ([6], [7] and others) uses the fact that the measured magnitude of the specific force of a still 3-axis accelerometer should be constant. Assuming  $N$  measurements and using (10) the calibration problem is equivalent to minimizing (11); this is typically done by employing the gradient descent method.

$$\begin{aligned} & \underset{\substack{T_a, h_a \\ f_k, k=1, 2, \dots, N}}{\text{minimize}} \sum_{k=1}^N \|y_{ak} - T_a f_k - h_a\|^2 \\ & \text{subject to } \|f_k\| = 1, \quad k = 1, 2, \dots, N \end{aligned} \quad (11)$$

A penalty function corresponding to (11) is

$$J = \sum_{k=1}^N \left\{ \|y_{ak} - T_a f_k - h_a\|^2 + \lambda \left( \|f_k\|^2 - 1 \right)^2 \right\} \quad (12)$$

where  $\lambda$  is a positive constant. It should be selected to balance the contribution of the two summands.<sup>4</sup>

In contrast to the magnetometer case, for the accelerometer's calibration we can find an initial estimate of the unknowns  $f$ ,  $T_a$  and  $h_a$ . Under the reasonable assumption of small scale-factor and cross-coupling errors, an initial estimate of  $T_a$  is the  $3 \times 3$  identity matrix.<sup>5</sup> In a similar way, bias vector  $h_a$  is initialized to the  $3 \times 1$  zero vector ( $0_{3 \times 1}$ ).

<sup>3</sup> $\varepsilon$  is assumed to be a zero mean random variable.

<sup>4</sup>Typically  $\lambda$  is selected to be in the order of  $\|T_a\|$

<sup>5</sup>This relates to the fact that we use  $\|f_k\| = 1$  and the assumption that the accelerometer's gain has been roughly pre-adjusted so that the specific force results in almost unit magnitude output.

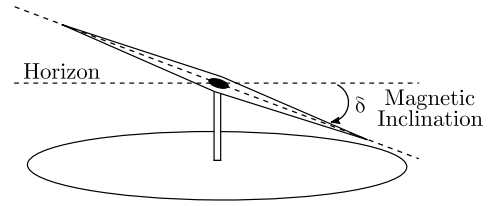


Fig. 2. Magnetic inclination.

Using the aforementioned initial estimate, the gradient descent method can minimize (12). However, as seen, optimization problem (11) share the same form with (3), the optimization problem derived for magnetometer calibration. Thus, magnetometer's calibration algorithm can also be used for accelerometer calibration as shown in Algorithm 2. Algorithm 2 is typically significantly faster in convergence and better in computational efficiency than the gradient descent one and this why it is preferred in our proposed calibration methodology here.

---

#### Algorithm 2: Accelerometer Calibration

---

- Step 1: Initialize  $f_k = \frac{y_{ak}}{\|y_{ak}\|}$ ,  $k = 1, 2, \dots, N$   
and form matrix  $G$
  - Step 2: Solve for  $L$  using least-squares:  
 $L = YG^T (GG^T)^{-1}$
  - Step 3: Extract  $T_a$  and  $h_a$  from  $L$
  - Step 4:  $\tilde{f}_k = T_a^{-1}(y_{ak} - h_a)$ ,  $k = 1, 2, \dots, N$
  - Step 5: Update  $G$  using  $f_k = \frac{\tilde{f}_k}{\|\tilde{f}_k\|}$ ,  $k = 1, 2, \dots, N$
  - Step 6: Calculate  $J$
  - Step 7: Repeat steps 2-6 until  $J$  is sufficiently small
- 

#### C. Recommended Calibration Procedure

In Subsections III-A and III-B, accelerometer's calibration is formulated as a mathematical problem identical to that of the magnetometer's calibration presented in Section II. Thus we recommend using the calibration sequence described in Figure 1 for accelerometer's calibration as well.

The performance characteristics of the accelerometer calibration algorithm are presented in Section VII.

### IV. ACCELEROMETER-MAGNETOMETER AXES ALIGNMENT

When accelerometer and magnetometer are combined for applications such as heading estimation, their axes must become aligned. A small misalignment between their axes is initially expected not only when the two sensors are in separate packages, but even when they are built into the same one. To compensate for this misalignment, the constant magnetic inclination during calibration is exploited.

#### A. Magnetic Inclination

Magnetic inclination (or magnetic dip, or dip angle) is the angle between the plane of the horizon and the Earth's

magnetic field lines as shown in Figure 2. Magnetic inclination varies with location. It can be defined by the inner product of the normalized gravity and the magnetic field vectors

$$\sin \delta = \frac{g^T m}{\|g\| \|m\|} \quad (13)$$

where  $\delta$  is the magnetic inclination angle,  $g$  is the gravity vector and  $m$  is the magnetic field vector.

### B. Axes Alignment Algorithm

If we have a calibrated accelerometer and a calibrated magnetometer, both fixed on a common rigid platform, we can use them to compute the inclination angle. To do so however, we have to align the axes of the two sensors, meaning that we have to derive a rotation matrix  $R$  ( $R \in SO(3)$ ) which rotates magnetometer's axes  $(x, y, z)$  into the accelerometer's axes  $(x, y, z)$  respectively. Note that for this to be possible, the two axes (coordinate) systems must have the same orientation. The derivation of the rotation matrix  $R$  and the inclination angle  $\delta$  is formulated as the following optimization problem

$$\begin{aligned} & \underset{R, \delta}{\text{minimize}} \quad \sum_{k=1}^N \left( \sin \delta - \frac{f_k^T R m_k}{\|f_k\| \|m_k\|} \right)^2 \\ & \text{subject to } R \in SO(3) \\ & \quad \delta \in \left[ -\frac{\pi}{2}, \frac{\pi}{2} \right] \end{aligned} \quad (14)$$

where  $\delta$  is the magnetic inclination angle,  $f$  and  $m$  are the calibrated accelerometer and magnetometer measurements respectively and  $R$  is a rotation matrix that rotates magnetometer's axes into the accelerometer's axes. Both inclination angle  $\delta$  and rotation matrix  $R$  are unknowns.

We form the vector  $x = [\text{vec}(R)^T \delta]^T$  and define a penalty function corresponding to (14) as

$$J(x) = \sum_{k=1}^N \left( \sin \delta - \frac{f_k^T R m_k}{\|f_k\| \|m_k\|} \right)^2 + \lambda \|RR^T - I\|_F^2 + \mu (\det R - 1)^2 \quad (15)$$

where  $\lambda$  and  $\mu$  are positive constants, selected to balance the contribution of the three summands. The gradient descent method [31] is used to minimize (15). The gradient is

$$\nabla J(x) = \begin{bmatrix} \frac{\partial J(x)}{\partial \text{vec}(R)} & \frac{\partial J(x)}{\partial \delta} \end{bmatrix}^T \quad (16)$$

where

$$\begin{aligned} \frac{\partial J(x)}{\partial \text{vec}(R)} &= -2 \sum_{k=1}^N \left[ \left( \sin \delta - \frac{f_k^T R m_k}{\|f_k\| \|m_k\|} \right) \frac{m_k \otimes f_k}{\|f_k\| \|m_k\|} \right] \\ & \quad + 4\lambda \text{vec} \left( RR^T R - R \right) \\ & \quad + 2\mu (\det(R) - 1) \text{vec} \left( \text{adj}(R)^T \right) \\ \frac{\partial J(x)}{\partial \delta} &= 2 \cos \delta \sum_{k=1}^N \left( \sin \delta - \frac{f_k^T R m_k}{\|f_k\| \|m_k\|} \right) \end{aligned}$$

and  $\otimes$  denotes the Kronecker's product [32].

An estimate of  $R$  for initializing the gradient descent algorithm is the  $3 \times 3$  identity matrix, assuming of a small misalignment between the axes of the two sensors. Inclination angle is initialized according to magnetic models (such as World Magnetic Model (WMM)) for the specific location on earth's surface,  $\delta = \delta_{WMM}$ .

The accelerometer and magnetometer axes alignment algorithm is described in Algorithm 3, where  $a$  and  $b$  are positive numbers for the line search.

---

### Algorithm 3: Accelerometer - Magnetometer Alignment

---

- Step 1: Initialize  $R = I_3$ ,  $\delta = \delta_{WMM}$ ,
  - Step 2: Initialize  $t$ ,  $a$  and  $b$
  - Step 3: Calculate the gradient:  
 $\Delta x = -\nabla J(x)$
  - Step 4: Choose step size:  
while  $J(x + t\Delta x) > J(x) + at\nabla J(x)^T \Delta x$   
 $t := bt$
  - Step 5: Update  $x = x + \Delta x$
  - Step 6: Calculate  $J(x)$
  - Step 7: Repeat steps 3-6 until  $J(x)$  is sufficiently small
- 

### C. Recommended Axes Alignment Procedure

In order for Algorithm 3 to result in accurate axes alignment between an accelerometer and a magnetometer, measurements of both sensors in multiple orientations are required. Thus, for axes alignment, we recommend the previously described magnetometer's calibration sequence (Figure 1) using both sensor's measurements. The evaluation of the described algorithm is presented in Section VII.

## V. GYROSCOPE CALIBRATION

This Section introduces a new approach to gyroscope calibration and provides the associated algorithm. It applies to the case where a 3-axis gyroscope, a 3-axis accelerometer and a 3-axis magnetometer are fixed on the same, rigid platform.

Assuming that the accelerometer and the magnetometer have already been calibrated and aligned, we use them to calculate the rotation of the platform between two still positions. The proposed approach is based on the fact that this rotation should be identical to that derived from the gyroscope, when the last one is also calibrated. Note that using the joint accelerometer - magnetometer rotation as reference for the gyroscope's calibration, the algorithm also aligns the axes of the gyroscope with those of the other two sensors.

Therefore, the new approach is comprised of a) the derivation of the rotation from the accelerometer and magnetometer data, b) the parametric derivation of the rotation from the gyroscope data, and, c) the optimization algorithm which equates the two of them.

### A. Rotation From Accelerometer and Magnetometer Data

Assume a rotation of the platform between two still positions. Let  $f_{begin}$  and  $f_{end}$  be the  $3 \times 1$  accelerometer's

measurement vectors before and after the rotation, while the platform is still. Similarly, let  $m_{begin}$  and  $m_{end}$  be the  $3 \times 1$  magnetometer's measurement vectors accordingly.

Assuming that  $f_{begin}$ ,  $f_{end}$ ,  $m_{begin}$  and  $m_{end}$  have been derived using calibrated accelerometer and magnetometer according to the proposed algorithms in Sections III and II, the angle between  $f_{begin}$  and  $m_{begin}$  is the same with the angle between  $f_{end}$  and  $m_{end}$  and all four vectors are of unit norm. The above allow us to use the TRIAD algorithm [33], [34] to find a rotation matrix  $R \in SO(3)$  such that  $Rf_{begin} = f_{end}$  and  $Rm_{begin} = m_{end}$ .

Given the unit vectors  $f_{begin}$ ,  $f_{end}$ ,  $m_{begin}$  and  $m_{end}$ , the TRIAD algorithm begins by constructing two triads of orthonormal column vectors according to

$$\begin{aligned} a_1 &= f_{begin}, \quad a_2 = (f_{begin} \times m_{begin}) / \|f_{begin} \times m_{begin}\| \\ a_3 &= (f_{begin} \times (f_{begin} \times m_{begin})) / \|f_{begin} \times m_{begin}\| \end{aligned}$$

and

$$\begin{aligned} b_1 &= f_{end}, \quad b_2 = (f_{end} \times m_{end}) / \|f_{end} \times m_{end}\| \\ b_3 &= (f_{end} \times (f_{end} \times m_{end})) / \|f_{end} \times m_{end}\| \end{aligned}$$

The matrix  $R$  is derived as

$$R = [b_1 \ b_2 \ b_3][a_1 \ a_2 \ a_3]^T$$

It is convenient to consider the application of the TRIAD algorithm as a function  $Ram$ , i.e.

$$R = Ram(f_{begin}, f_{end}, m_{begin}, m_{end}) \quad (17)$$

### B. Rotation From Gyroscope Data

Using  $K$  sequential gyroscope's measurements sampled at rate  $\tau_s$ , we can calculate the rotation matrix representing the sensor's body frame rotation from time  $t$  to time  $t + K\tau_s$ . Let  $\omega_k = [\omega_{xk} \ \omega_{yk} \ \omega_{zk}]^T$  be the  $k^{th}$  sample of the gyroscope's output. Using the entries of  $\omega_k$ , we define the skew symmetric matrix function

$$\Omega(\omega_k) = \begin{bmatrix} 0 & -\omega_{zk} & \omega_{yk} \\ \omega_{zk} & 0 & -\omega_{xk} \\ -\omega_{yk} & \omega_{xk} & 0 \end{bmatrix}. \quad (18)$$

Setting  $\bar{\omega} = [\omega_1 \ \omega_2 \ \dots \ \omega_K] \in \mathbb{R}^{3 \times K}$ , the rotation matrix from  $t$  to  $t + K\tau_s$  can be approximated by the outcome of the following function [5], [30]

$$R_g(\bar{\omega}) = (I + \tau_s \Omega(\bar{\omega}e_1))(I + \tau_s \Omega(\bar{\omega}e_2)) \dots (I + \tau_s \Omega(\bar{\omega}e_K)) \quad (19)$$

where  $e_k$  is the  $k^{th}$  normal vector in  $\mathbb{R}^K$ .

### C. Measurement Model

Gyroscope's measurement is modeled as [5], [30]

$$y_g = \omega + T_{sf}\omega + T_{cc}\omega + h_g + \varepsilon, \quad (20)$$

where  $y_g$  is the  $3 \times 1$  measurement vector,  $\omega$  is the  $3 \times 1$  true angular velocity vector,  $T_{sf}$  is a  $3 \times 3$  diagonal matrix representing the linear scale-factor error of the sensor,  $T_{cc}$  is a  $3 \times 3$  matrix representing the cross-coupling error,  $h_g$  is

the  $3 \times 1$  gyroscope's bias vector and  $\varepsilon$  is the measurement's random error.<sup>6</sup> Defining  $T_g = I_3 + T_{sf} + T_{cc}$ , (20) can be written as

$$y_g = T_g\omega + h_g + \varepsilon \quad (21)$$

### D. Calibration Algorithm

Assume that the sensor's platform rotates  $N$  times with a short period of stillness between them. During every rotation, the gyroscope is regularly sampled every  $\tau_s$  seconds and the samples are recorded. Recording begins from the still position, just before the rotation begins, and ends at the next still position, just after the rotation ends. We also assume that every one of the three gyroscope's axes is rotated significantly in at least one of the rotations.

Let  $\omega_j^n$  be the  $j^{th}$  gyroscope's sample measured sample (i.e.  $y_g$  in (21)) during the  $n^{th}$  rotation,  $n = 1, 2, \dots, N$ . Using (21), we get the calibrated sample

$$\tilde{\omega}_j^n = H_g(\omega_j^n - h_g)$$

where  $H_g = T_g^{-1}$ . Here we assume that  $T_g$  is invertible. This is a rational assumption as a non-invertible  $T_g$  would imply that not all three axes are expressed in the output of the sensor. For every rotation, we form the matrix

$$\bar{\omega}^n = [\tilde{\omega}_1^n \ \tilde{\omega}_2^n \ \dots \ \tilde{\omega}_{M_n}^n]$$

where  $M_n$  is the number of the recorded samples during the  $n^{th}$  rotation. Then, using (19), for every rotation, we derive a rotation matrix as a function of the calibration parameters  $H_g$  and  $h_g$  in (21).

$$R_g^n = R_g(\bar{\omega}^n) \quad (22)$$

Calculating the rotations using accelerometer's and magnetometer's measurements, as in Section V-A, requires measurements of both sensors before and after every rotation, while the sensors are still. Let  $f_{begin}^n$  and  $f_{end}^n$  be the measured specific force vectors exactly before and after rotation  $n$ ,  $n = 1, 2, \dots, N$ . Similarly let  $m_{begin}^n$  and  $m_{end}^n$  be the corresponding vectors of the magnetic field. To minimize the effect of the sensors' noise, we prefer to define the above four vectors as the average of  $L$  samples. Then, using (17), for every rotation, we derive the accelerometer-magnetometer rotation matrix

$$R_{am}^n = Ram(f_{begin}^n, f_{end}^n, m_{begin}^n, m_{end}^n). \quad (23)$$

To calibrate the gyroscope we minimize the mean square error between the rotation calculated using gyroscope's measurements  $R_g^n$  and the corresponding rotation calculated using accelerometer's and magnetometer's measurements  $R_{am}^n$ . This is done for all  $N$  rotations simultaneously, and so the calibration procedure can be posed as the minimization of cost function  $J(x)$ , where

$$J(x) = \sum_{n=1}^N \left\{ \|R_{am}^n - R_g^n\|^2 \right\} + \lambda \|H_g(\omega_{still} - h_g)\|^2 \quad (24)$$

<sup>6</sup> $\varepsilon$  is assumed to be a zero mean random variable.

and

$$x = [\text{vec}(H_g)^T h_g^T]^T$$

The positive constant  $\lambda$  is selected to balance the contribution of the two summands in (24) where the second one is for nulling the sensor's bias. Note that  $\omega_{still}$  is the gyroscope's output ( $y_g$  in (21)) when it is still (i.e.  $\omega = 0$  in (21)), also defined as the average of  $M$  measurements to reduce random noise.

We solve (24) using the gradient descent method with the gradient of  $J(x)$  be numerically calculated. Assuming small scale-factor, cross-coupling and bias errors we initialize  $H_g$  to the  $3 \times 3$  identity matrix and  $h_g$  to the  $3 \times 1$  zero vector.

Gyroscope calibration algorithm is shown in Algorithm 4, where  $a$  and  $b$  are positive numbers for the line search.

---

**Algorithm 4:** Gyroscope Calibration
 

---

- Step 1: Initialize  $H_g = I_3$ ,  $h_g = 0_{3 \times 1}$ ,  
 Step 2: Initialize  $t, a$  and  $b$   
 Step 3: Calculate the gradient:  
 $\Delta x = -\nabla J(x)$   
 Step 4: Choose step size:  
 while  $J(x + t\Delta x) > J(x) + at\nabla J(x)^T \Delta x$   
 $t := bt$   
 Step 5: Update  $x = x + \Delta x$   
 Step 6: Calculate  $J(x)$   
 Step 7: Repeat steps 3-6 until  $J(x)$  is sufficiently small
- 

### E. Recommended Calibration Procedure

For the gyroscope's calibration we must calculate the calibration matrix  $H_g$  and the offset vector  $h_g$ . So, in total there are 12 unknowns. These unknowns are calculated by minimizing (ideally zero) the cost function  $J(x)$  in (24). Setting  $J(x)$  equal to zero is equivalent to

$$R_{am}^n = R_g^n, \quad n = 1, 2, \dots, N \quad (25)$$

and

$$\omega_{still} = h_g \quad (26)$$

where  $N$  is the number of rotations.

In an intuitive way, the number of rotations required can be derived as follows. Since  $R_{am}^n$  and  $R_g^n$  are by default rotation matrices, (25) contributes 3 scalar equations for each rotation. From (26) we have another 3 scalar equations. Thus in total we have  $3N + 3$  scalar equations, implying that  $N = 3$  is the minimum number of rotations needed to balance the unknowns with the equations.

To achieve accurate calibration of the gyroscope using Algorithm 4, every one of the three gyroscope's axes must rotate significantly in at least one of the rotations. The exact form of the rotations is not critical otherwise. As a guidance for choosing the rotation pattern, the sequence in Figure 3 is recommended. In Figure 3, the  $(X, Y, Z)$  coordinate system denotes the sensor's body frame and the  $(\tilde{X}, \tilde{Y}, \tilde{Z})$  coordinate

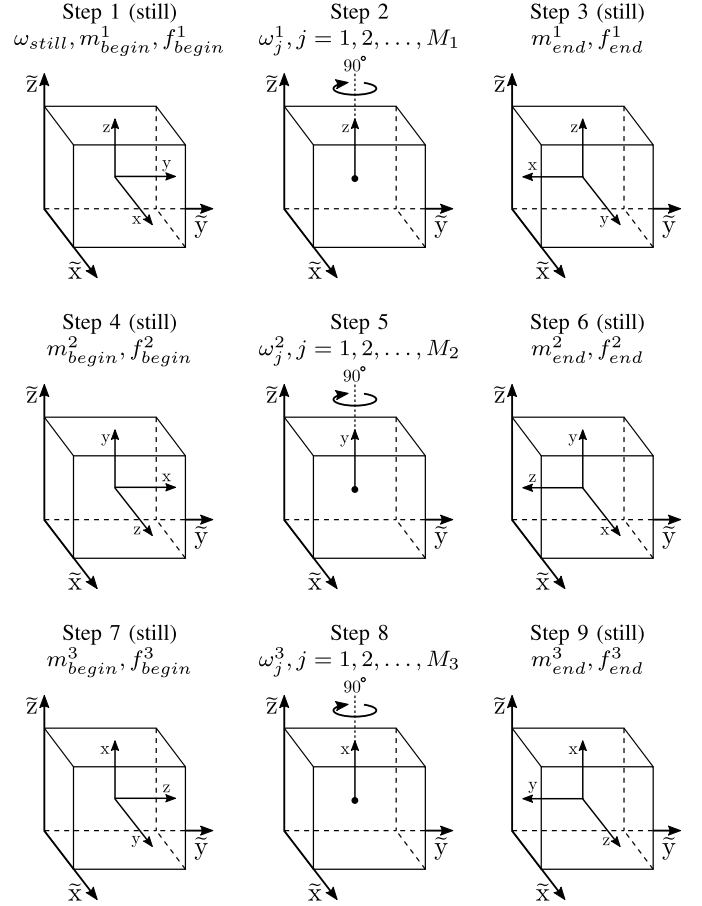


Fig. 3. Recommended sequence of approximate orientations and rotations for gyroscope calibration.

system denotes the calibration reference frame which is fixed. Note that the steps in Figure 3 should not be confused with the steps of the Algorithm 4.

**Important Note:** All rotations are **approximately**  $90^\circ$  (e.g. between  $60^\circ$  and  $120^\circ$ ). Keeping the sensor platform still between the rotations is important.

Gyroscope calibration algorithm is evaluated using experimental data. Its performance is presented in Section VII.

## VI. MAG.I.C.AL. METHODOLOGY

In this section, we describe MAG.I.C.AL. methodology as a complete procedure for joint calibration of a 3-axis accelerometer, a 3-axis magnetometer and a 3-axis gyroscope. MAG.I.C.AL. comprises of the previously presented sub-processes for magnetometer calibration (Section II), accelerometer calibration (Section III), accelerometer and magnetometer axes alignment (Section IV), and gyroscope calibration (Section V).

The 15-step MAG.I.C.AL. calibration procedure, integrating all the presented sub-processes into a unified algorithm, is shown in Figure 4. The steps of the procedure are grouped in Table I according to their use in each of the sub-processes.

In Figure 4, the  $(X, Y, Z)$  coordinate system denotes the sensor's body frame and the  $(\tilde{X}, \tilde{Y}, \tilde{Z})$  coordinate system denotes the calibration reference frame which is fixed.

TABLE I  
REQUIRED STEPS FOR EACH MAG.I.C.AL SUB-PROCESS

Sub-Process	Steps
Magnetometer Calibration	1,3,4,5,6,8,9,10,11,13,14,15
Accelerometer Calibration	1,3,4,5,6,8,9,10,11,13,14,15
Magnetometer - Accelerometer Axes Alignment	1,3,4,5,6,8,9,10,11,13,14,15
Gyroscope Calibration	1,2,3,6,7,8,11,12,13

**Important Note:** The orientation of the sensor in meant to be **approximate**. Orientation and placement of the sensor can be done by hand with an accuracy of say  $\pm 15^\circ$  of Euler angle. Also, all rotations are **approximately**  $90^\circ$  (e.g. between  $60^\circ$  and  $120^\circ$ ).

## VII. EXPERIMENTAL RESULTS AND EVALUATION

In order to evaluate MAG.I.C.AL., an inertial measurement unit (IMU) & magnetometer device (unified platform) was developed based on Bosch Sensortec BNO055. The specifications of the BNO055 SoC are given in [35]. Using it we performed the calibration sequence in Figure 4 five times and each time we recorded the corresponding dataset. We applied MAG.I.C.AL. to each one of the five datasets and derived five sets of calibration parameters respectively. Then, we used the last ones to analyze the stability and the repeatability, and estimate the accuracy of the MAG.I.C.AL. methodology. The results are discussed in the following subsections.

### A. Convergence

In this section we examine the convergence of the MAG.I.C.AL. methodology using the five aforementioned datasets. Figures 5–8 present the convergence of each sub-process of the methodology for each dataset.

As seen in Figure 5, the cost function of the accelerometer's calibration sub-process appears to be monotonic and requires only a few iterations of the proposed algorithm to converge.

In Figure 6 the convergence of the magnetometer's calibration sub-process is presented. Although the required iterations and the shape of the cost function are very different for each dataset, the algorithm converges monotonically for all five datasets.

The cost function of the accelerometer's and magnetometer's axes alignment sub-process also appears to be monotonic as seen in Figure 7. The algorithm converges for all five datasets.

Gyroscope calibration algorithm converges after only a few iterations for all five datasets, as seen in Figure 8. The corresponding cost function appears to be monotonic.

### B. Measuring Distance Between Calibration Parameter Sets

Applying the calibration methodology to all five datasets, we expect some consistency between the calibration parameters derived from them. The calibration parameter sets of the magnetometer, the accelerometer and the gyroscope are pairs of a calibration matrix and an offset vector,  $(T_m, h_m)$ ,  $(T_a, h_a)$  and  $(T_g, h_g)$  as shown in (2), (10) and (21) respectively.

The offset vectors are defined uniquely in the proposed algorithms, in the sense that they are independent of the true

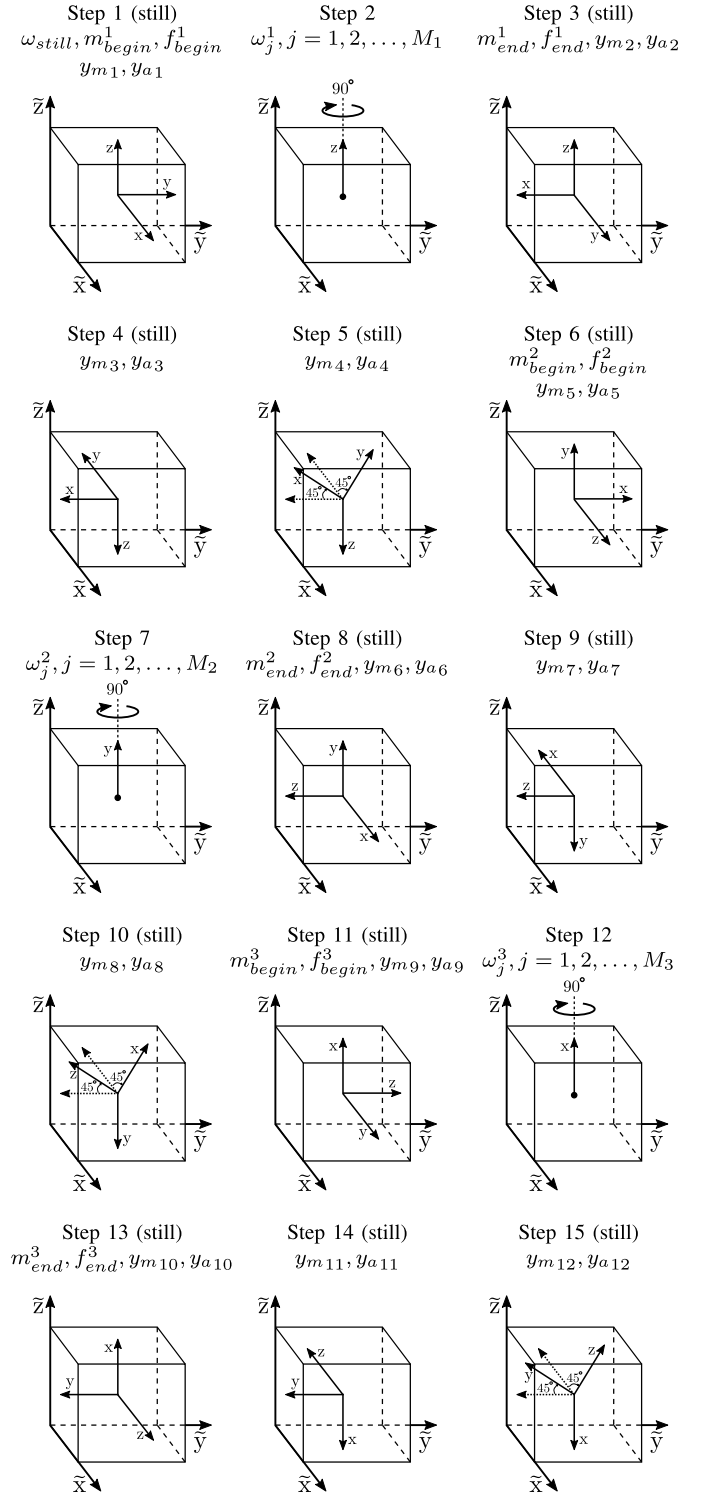


Fig. 4. MAG.I.C.AL. recommended sequence of approximate orientations and rotations.

values of the magnetic field, the specific force and the angular velocity respectively. Therefore, the distance between offset vectors derived using different datasets can be defined as the norm of their algebraic difference, i.e.  $d(x_i, x_j) = \|x_i - x_j\|$ .

The normalized distance  $\bar{d}$  is defined as the ratio of the average distance divided by the average norm of the vectors, i.e. for  $N$  datasets ( $N = 5$  here) there are  $\binom{N}{2}$  pairs and  $\bar{d}$  is

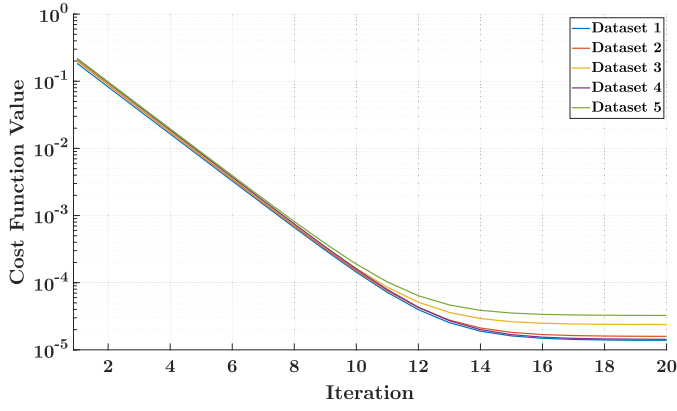


Fig. 5. Convergence of accelerometer calibration algorithm.

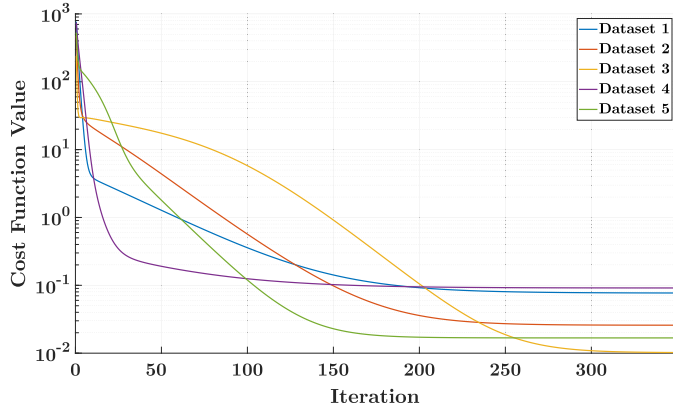


Fig. 6. Convergence of magnetometer calibration algorithm.

given by

$$\bar{d}(x_1, x_2, \dots, x_N) = \frac{\left( \sum_{1 \leq i < j \leq N} d(x_i, x_j) \right) / \binom{N}{2}}{\left( \sum_{1 \leq i \leq N} \|x_i\| \right) / N}.$$

For the vectors sets  $h_m$ ,  $h_a$  and  $h_g$  we calculated the distance  $\bar{d}$  based on the five datasets. It is

$$\begin{aligned} \bar{d}(h_{m1}, h_{m2}, \dots, h_{m5}) &= 0.0208 \\ \bar{d}(h_{a1}, h_{a2}, \dots, h_{a5}) &= 0.0393 \\ \bar{d}(h_{g1}, h_{g2}, \dots, h_{g5}) &= 0.0480 \end{aligned} \quad (27)$$

Defining the distance between calibration matrices derived using different datasets is more tricky because the proposed algorithms consider the true values of the magnetic field, the specific force and angular velocity to be unknowns. The last ones are derived along with the calibration matrices to minimize the random errors in (2), (10) and (21) respectively.

Observe for example in (2) that if we replace  $T_m$  with  $T_m Q$  and  $m$  with  $Q^T m$ , where  $Q$  is an orthogonal  $3 \times 3$  matrix, i.e.  $Q \in O(3)$ , the resulting measurement  $y_m$  is unaltered. The same is true for (10) and (21).

Therefore the calibration matrices are derived subject to orthogonal multiplication uncertainty. To this end we

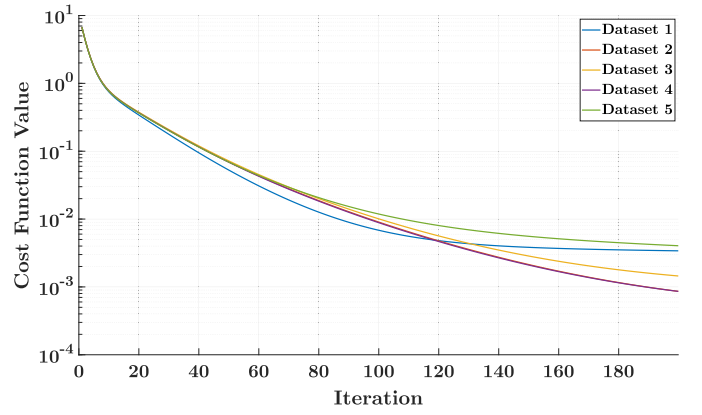


Fig. 7. Convergence of axes alignment algorithm.

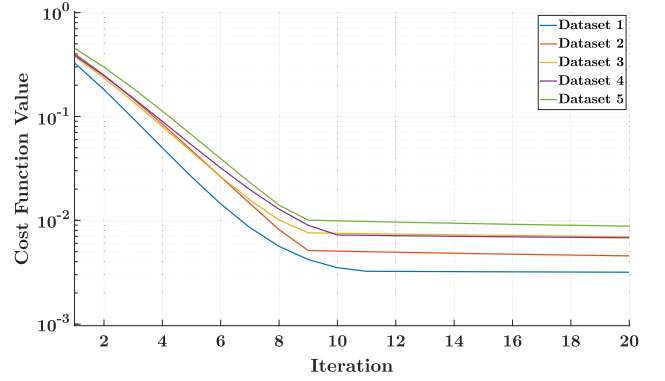


Fig. 8. Convergence of gyroscope calibration algorithm.

define the distance between two calibration matrices (of the accelerometer, the magnetometer or the gyroscope) derived from different datasets as follows.

*Definition 1:* The distance between two  $3 \times 3$  calibration matrices  $T_1$  and  $T_2$  can be defined as:

$$D(T_1, T_2) = \min_{Q \in O(3)} \|QT_1 - T_2\|_F \quad (28)$$

The minimizing matrix  $Q$  can be calculated using the orthogonal Procrustes Theorem [36].

Similarly to the offset vectors, the normalized distance  $\bar{D}$  between  $N$  calibration matrices is defined as

$$\bar{D}(X_1, X_2, \dots, X_N) = \frac{\left( \sum_{1 \leq i < j \leq N} D(X_i, X_j) \right) / \binom{N}{2}}{\left( \sum_{1 \leq i \leq N} \|X_i\|_F \right) / N}. \quad (29)$$

For the calibration matrix sets  $T_m$ ,  $T_a$  and  $T_g$  we calculated the distance  $\bar{D}$  based on five datasets. It is

$$\begin{aligned} \bar{D}(T_{m1}, T_{m2}, \dots, T_{m5}) &= 0.0287 \\ \bar{D}(T_{a1}, T_{a2}, \dots, T_{a5}) &= 0.0018 \\ \bar{D}(T_{g1}, T_{g2}, \dots, T_{g5}) &= 0.0222 \end{aligned} \quad (30)$$

Functions  $d(\cdot, \cdot)$  and  $D(\cdot, \cdot)$  represent the distance among the offset vectors and the distance among the calibration matrices derived from different datasets respectively. Thus,

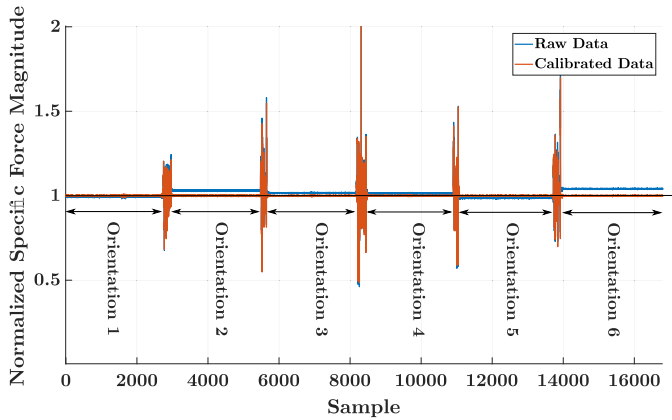


Fig. 9. Normalized magnitude of raw and calibrated accelerometer measurements in six still orientations.

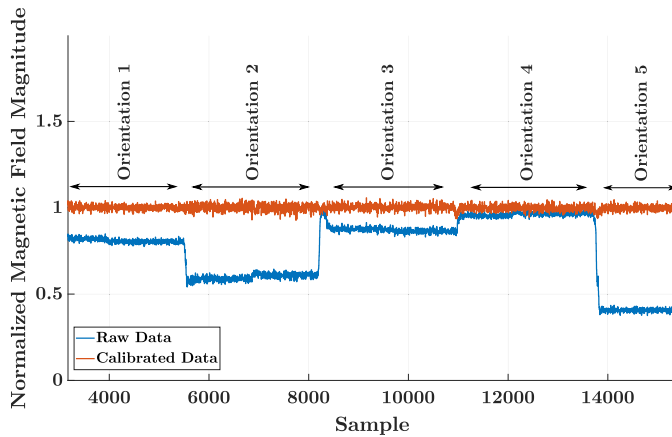


Fig. 10. Normalized magnitude of raw and calibrated magnetometer measurements in five still orientations.

the small values of the normalized average distances (27) and (30) indicate good repeatability of the proposed calibration algorithm i.e. the algorithm return similar calibration parameters for different dataset inputs.

### C. Calibration Results

For accelerometer and magnetometer, the effectiveness of the calibration algorithms can be deduced from the true values of the specific force  $\tilde{f}$  and the magnetic field  $\tilde{m}$  having unit magnitude. In Figures 9 and 10 the normalized magnitude of both raw and calibrated accelerometer and magnetometer measurements are presented.

In the accelerometer-magnetometer axes alignment algorithm, except from the rotation matrix  $R$ , the algorithm also derives the magnetic inclination angle. If both sensors are calibrated and their axes are aligned, the calculated inclination angle should be close to that given by magnetic models such as World Magnetic Model (WMM) and Enhanced Magnetic Model (EMM).

The experimental calibration measurements took place inside the campus of the National Technical University of Athens. According to WMM the magnetic inclination angle at the location of the experiment is  $54.6025^\circ$ . The values derived from the axes alignment algorithm are presented at Table II.

As seen in Table II, the measured inclination angles have a maximum deviation of 0.52% from the value given by

TABLE II  
MAGNETIC INCLINATION ANGLE CALCULATED BY AXES ALIGNMENT ALGORITHM FOR EACH DATASET

Dataset	Magnetic Inclination
1	$54.38^\circ$
2	$54.48^\circ$
3	$54.32^\circ$
4	$54.43^\circ$
5	$54.41^\circ$

TABLE III  
MEASURED ROLL ANGLE FOR  $90^\circ$  ROTATION ABOUT X-AXIS

Rotation	Roll Angle
1	$90.348^\circ$
2	$89.769^\circ$
3	$90.216^\circ$
4	$90.402^\circ$
5	$89.976^\circ$

the WMM. This indicates a fine alignment between the two sensors.

To assess the performance of the gyroscope calibration algorithm, we rotated the device by  $90^\circ$ , about its x-axis five times. The corresponding Euler angle derived from the measurements for each rotation is presented in table III.

The measured Euler angles in Table III are very close to the true rotation angle ( $90^\circ$ ) indicating the good accuracy of the proposed calibration algorithm without using any special piece of equipment and without any external attitude reference.

## VIII. CONCLUSION

In this paper we introduced MAG.I.C.AL., a novel, unified methodology and the corresponding algorithm for calibration and axes alignment of a 3-axis magnetometer, a 3-axis accelerometer a 3-axis gyroscope. MAG.I.C.AL. performs very well in terms of convergence, repeatability and computational efficiency. MAG.I.C.AL. is applied by following a simple sequence of fifteen approximate orientations and rotations (possibly made by hand) without the need of any external piece of equipment. MAG.I.C.AL. is tested using experimental measurements. The experimental results demonstrated good convergence and repeatability of the algorithm and its capability of accurately determining the calibration parameters of the three sensors. Additional material including datasets and implementations of the algorithms are available on the website <http://magical.circuits.ece.ntua.gr>.

## REFERENCES

- [1] Z. Li, C. Song, J. Cai, R. Hua, and P. Yu, "An improved pedestrian navigation system using IMU and magnetometer," in *Proc. Int. Conf. Comput. Syst., Electron. Control (ICCSEC)*, Dec. 2017, pp. 1639–1642.
- [2] R. Stirling, J. Collin, K. Fyfe, and G. Lachapelle, "An innovative shoe-mounted pedestrian navigation system," in *Proc. Eur. Navigat. Conf. GNSS*, vol. 110, no. 5, Apr. 2003.
- [3] W. Li and J. Wang, "Effective adaptive Kalman filter for MEMS-IMU/magnetometers integrated attitude and heading reference systems," *J. Navigat.*, vol. 66, no. 1, pp. 99–113, 2013.

- [4] S. O. H. Madgwick, A. J. L. Harrison, and R. Vaidyanathan, "Estimation of IMU and MARG orientation using a gradient descent algorithm," in *Proc. IEEE Int. Conf. Rehabil. Robot.*, Jun./Jul. 2011, pp. 1–7.
- [5] P. D. Groves, *Principles of GNSS, Inertial, and Multisensor Integrated Navigation Systems*. Norwood, MA, USA: Artech House, 2013.
- [6] X. Lu, Z. Liu, and J. He, "Maximum likelihood approach for low-cost MEMS triaxial accelerometer calibration," in *Proc. 8th Int. Conf. Intell. Hum.-Mach. Syst. Cybern. (IHMSC)*, vol. 1, Aug. 2016, pp. 179–182.
- [7] N. Ammann, A. Derksen, and C. Heck, "A novel magnetometer-accelerometer calibration based on a least squares approach," in *Proc. Int. Conf. Unmanned Aircr. Syst. (ICUAS)*, Jun. 2015, pp. 577–585.
- [8] Y. Zhong, Y. Xu, N. He, and X. Yu, "A new drone accelerometer calibration method," in *Proc. 37th Chin. Control Conf. (CCC)*, Jul. 2018, pp. 9928–9933.
- [9] M. Glueck, A. Buhmann, and Y. Manoli, "Autocalibration of MEMS accelerometers," in *Proc. IEEE Int. Instrum. Meas. Technol. Conf.*, May 2012, pp. 1788–1793.
- [10] I. Frosio, F. Pedersini, and N. A. Borghese, "Autocalibration of MEMS accelerometers," *IEEE Trans. Instrum. Meas.*, vol. 58, no. 6, pp. 2034–2041, Jun. 2009.
- [11] Q. Tang, X. Wang, Q. Yang, and C. Liu, "An improved scale factor calibration model of MEMS gyroscopes," in *Proc. IEEE Int. Instrum. Meas. Technol. Conf. (I2MTC)*, May 2014, pp. 752–755.
- [12] S. Nadig, V. Pinrod, S. Ardanuç, and A. Lal, "In-run scale factor and drift calibration of MEMS gyroscopes with rejection of acceleration sensitivities," in *Proc. IEEE Int. Symp. Inertial Sens. Syst.*, Feb. 2016, pp. 144–145.
- [13] J. Zhang *et al.*, "A novel scale factor calibration method for a MEMS gyroscope based on virtual coriolis force," in *Proc. 10th IEEE Int. Conf. Nano/Micro Eng. Mol. Syst.*, Apr. 2015, pp. 58–62.
- [14] Z. F. Syed, P. Aggarwal, C. Goodall, X. Niu, and N. El-Sheimy, "A new multi-position calibration method for MEMS inertial navigation systems," *Meas. Sci. Technol.*, vol. 18, no. 7, p. 1897, 2007. [Online]. Available: <http://stacks.iop.org/0957-0233/18/i=7/a=016>
- [15] U. Qureshi and F. Golnaraghi, "An algorithm for the in-field calibration of a MEMS IMU," *IEEE Sensors J.*, vol. 17, no. 22, pp. 7479–7486, Nov. 2017.
- [16] Y. Wu and L. Pei, "Gyroscope calibration via magnetometer," *IEEE Sensors J.*, vol. 17, no. 16, pp. 5269–5275, Aug. 2017.
- [17] R. Alonso and M. D. Shuster, "TWOSTEP: A fast robust algorithm for attitude-independent magnetometer-bias determination," *J. Astron. Sci.*, vol. 50, no. 4, pp. 433–451, 2002.
- [18] Y. Wu and W. Shi, "On calibration of three-axis magnetometer," *IEEE Sensors J.*, vol. 15, no. 11, pp. 6424–6431, Nov. 2015.
- [19] M. Kok and T. B. Schön, "Maximum likelihood calibration of a magnetometer using inertial sensors," *IFAC Proc. Volumes*, vol. 47, no. 3, pp. 92–97, 2014.
- [20] M. Kok and T. B. Schön, "Magnetometer calibration using inertial sensors," *IEEE Sensors J.*, vol. 16, no. 14, pp. 5679–5689, Jul. 2016.
- [21] J. F. Vasconcelos *et al.*, "Geometric approach to strapdown magnetometer calibration in sensor frame," *IEEE Trans. Aerosp. Electron. Syst.*, vol. 47, no. 2, pp. 1293–1306, Apr. 2011.
- [22] E. Dorveaux, D. Vissière, A.-P. Martin, and N. Petit, "Iterative calibration method for inertial and magnetic sensors," in *Proc. 48th IEEE Conf. Decis. Control (CDC)*, Dec. 2009, pp. 8296–8303.
- [23] Y. Wu, D. Zou, P. Liu, and W. Yu, "Dynamic magnetometer calibration and alignment to inertial sensors by Kalman filtering," *IEEE Trans. Control Syst. Technol.*, vol. 26, no. 2, pp. 716–723, Mar. 2018.
- [24] M. Kok, J. D. Hol, T. B. Schön, F. Gustafsson, and H. Luinge, "Calibration of a magnetometer in combination with inertial sensors," in *Proc. 15th Int. Conf. Inf. Fusion*, Jul. 2012, pp. 787–793.
- [25] M. V. Gheorghe, "Calibration for tilt-compensated electronic compasses with alignment between the magnetometer and accelerometer sensor reference frames," in *Proc. IEEE Int. Instrum. Meas. Technol. Conf. (I2MTC)*, May 2017, pp. 1–6.
- [26] Y. Wu and S. Luo, "On misalignment between magnetometer and inertial sensors," *IEEE Sensors J.*, vol. 16, no. 16, pp. 6288–6297, Aug. 2016.
- [27] H. Zhang, Y. Wu, W. Wu, M. Wu, and X. Hu, "Improved multi-position calibration for inertial measurement units," *Meas. Sci. Technol.*, vol. 21, no. 1, 2010, Art. no. 015107. [Online]. Available: <http://stacks.iop.org/0957-0233/21/i=1/a=015107>
- [28] J. Metge, R. Mégret, A. Giremus, Y. Berthoumieu, and T. Décamps, "Calibration of an inertial-magnetic measurement unit without external equipment, in the presence of dynamic magnetic disturbances," *Meas. Sci. Technol.*, vol. 25, no. 12, 2014, Art. no. 125106. [Online]. Available: <http://stacks.iop.org/0957-0233/25/i=12/a=125106>
- [29] G. Strang, *Linear Algebra and its Applications*. Pacific Grove, CA, USA: Brooks/Cole, 2007.
- [30] A. Noureldin, T. B. Karamat, and J. Geogy, *Fundamentals of Inertial Navigation, Satellite-Based Positioning and Their Integration*. Berlin, Germany: Springer-Verlag, 2013.
- [31] S. Boyd and L. Vandenberghe, *Convex Optimization*. Cambridge, U.K.: Cambridge Univ. Press, 2013.
- [32] R. A. Horn and C. R. Johnson, *Matrix Analysis*. Cambridge, U.K.: Cambridge Univ. Press, 2013.
- [33] H. D. Black, "A passive system for determining the attitude of a satellite," *AIAA J.*, vol. 2, no. 7, pp. 1350–1351, Jul. 1964. doi: [10.2514/3.2555](https://doi.org/10.2514/3.2555).
- [34] M. D. Shuster and S. D. Oh, "Three-axis attitude determination from vector observations," *J. Guid., Control, Dyn.*, vol. 4, no. 1, pp. 70–77, Jan. 1981. doi: [10.2514/3.19717](https://doi.org/10.2514/3.19717).
- [35] *BNO055—Intelligent 9-Axis Absolute Orientation Sensor*, document BST-BNO055-DS000-14, 1.4, Bosch Sensortec, Kusterdingen, Germany, Jun. 2016. [Online]. Available: [https://aebst.resource.bosch.com/media\\_tech/media/datasheets/BST-BNO055-DS000.pdf](https://aebst.resource.bosch.com/media_tech/media/datasheets/BST-BNO055-DS000.pdf)
- [36] P. H. Schönemann, "A generalized solution of the orthogonal procrustes problem," *Psychometrika*, vol. 31, no. 1, pp. 1–10, Mar. 1966.



**Konstantinos Papafotis** (S'19) received the Diploma degree in electrical and computer engineering from the National Technical University of Athens, Greece, in 2015, where he is currently pursuing the Ph.D. degree, under the supervision of Prof. P. P. Sotiriadis.

He is a Teaching Assistant in several undergraduate courses and acts as an Advisor of several diploma theses. He has authored several conference papers and one journal article. His main research interests include inertial navigation, embedded systems, and wireless sensor's systems. He has received the Best Paper Award from the IEEE International Conference on Modern Circuits and Systems Technologies in 2019. He is a regular reviewer of many IEEE publications.



**Paul P. Sotiriadis** (SM'18) received the Diploma degree in electrical and computer engineering from the National Technical University of Athens, the M.S. degree in electrical engineering from Stanford University, CA, USA, and the Ph.D. degree in electrical engineering and computer science from the Massachusetts Institute of Technology, Cambridge, USA, in 2002.

He is a Faculty Member of the Electrical and Computer Engineering Department, National Technical University of Athens, Greece, and the Director of the Electronics Laboratory. In 2002, he joined Johns Hopkins University as an Assistant Professor of Electrical and Computer Engineering. In 2012, he joined the Faculty of the Electrical and Computer Engineering Department, National Technical University of Athens. He has authored or coauthored over 130 technical papers in IEEE journals and conferences. He holds one patent. He has several patents pending, and he has contributed chapters to technical books. His research interests include design, optimization, and the mathematical modeling of analog and mixed-signal circuits, RF and microwave circuits, advanced frequency synthesis, biomedical instrumentation, and interconnect networks in deep-submicrometer technologies. He has led several projects in his research fields supported by U.S. organizations, and he has collaborations with industry and national labs. He has received several awards including the 2012 Guillemin-Cauer Award from the IEEE Circuits and Systems Society, the Best Paper Award from the IEEE International Symposium on Circuits and Systems in 2007, the Best Paper Award from the IEEE International Frequency Control Symposium in 2012, and the Best Paper Award from the IEEE International Conference on Modern Circuits and Systems Technology in 2019.

Dr. Sotiriadis has been a member of technical committees of many conferences. He is an Associate Editor of the IEEE TRANSACTIONS ON CIRCUITS AND SYSTEMS-I and the IEEE SENSORS JOURNAL. He has served as an Associate Editor for the IEEE TRANSACTIONS ON CIRCUITS AND SYSTEMS-II from 2005 to 2010. He is regular reviewer of many IEEE TRANSACTIONS and conferences, and he serves on proposal review panels.